ORNL/TM-2021/2264

Fracture Toughness and Fatigue Crack Growth Rate Testing of Baffle-Former Bolts Harvested from a Westinghouse Two-Loop Downflow Type PWR

Xiang (Frank) Chen
Mikhail A. Sokolov

September 2021

OAK RIDGE National Laboratory

ORNL IS MANAGED BY UT-BATTELLE LLC FOR THE US DEPARTMENT OF ENERGY

ORNL/TM-2021/2264

Light Water Reactor Sustainability (LWRS) Program
M2LW-21OR0402053

FRACTURE TOUGHNESS AND FATIGUE CRACK GROWTH RATE TESTING OF BAFFLE-FORMER BOLTS HARVESTED FROM A WESTINGHOUSE TWO-LOOP DOWNFLOW TYPE PWR

Xiang (Frank) Chen, Mikhail A. Sokolov

Materials Science and Technology Division
Oak Ridge National Laboratory

September 2021

Prepared by
OAK RIDGE NATIONAL LABORATORY
Oak Ridge, TN 37831-6283
managed by
UT-BATTELLE LLC
for the
US DEPARTMENT OF ENERGY
under contract DE-AC05-00OR22725

This page intentionally left blank

CONTENTS

LIST OF FIGURES

LIST OF TABLES

This page intentionally left blank

ACKNOWLEDGEMENTS

This research was sponsored by the U.S. Department of Energy, Office of Nuclear Energy, Light Water Reactor Sustainability Program, Materials Research Pathway, under contract DE-AC05-00OR22725 with UT-Battelle, LLC/Oak Ridge National Laboratory (ORNL). The authors wish to thank Thomas M. Rosseel for the programmatic support for this project.

The authors extend their appreciation to Mark Delph, Clay Morris, and other team members at Irradiated Materials Examination and Testing Facility at ORNL for their support during hot cell testing. The authors would like to thank Eric Manneschmidt of ORNL for his technical support for test fixture design and in-cell installation. The authors are grateful to Dr. Lizhen Tan and Dr. Maxim Gussev from ORNL for their technical review of this report. We acknowledge Heather Malikowski and Robert Marcello of Exelon Corporation and Bernard Rudell formerly of Exelon Corporation for their assistance during the bolt harvesting process. Lastly, we would like to thank the late Mike Burke formerly with Electrical Power Research Institute who led the sample preparation, machining, and shipping when he was working at Westinghouse.

This page intentionally left blank

EXECUTIVE SUMMARY

As one of the pressurized water reactor (PWR) internal components, baffle-former bolts (BFBs) are subjected to significant mechanical stress and neutron irradiation from the reactor core during the plant operation. Over the long operation period, these conditions lead to potential degradation and reduced load-carrying capacity of the bolts. In support of evaluating long-term operational performance of materials used in core internal components, the Oak Ridge National Laboratory (ORNL), through the Department of Energy (DOE), Light Water Reactor Sustainability (LWRS) Program, Materials Research Pathway (MRP) has harvested two high fluence BFBs from a commercial Westinghouse two-loop downflow type PWR. The two bolts of interest, i.e. bolts # 4412 and 4416, were withdrawn from service in 2011 as part of a preventative replacement plan. No identification of cracking or potential damage was found for these bolts during their removal in 2011. However, the bolts required a lower torque for removal from the baffle structure than the original torque specified during installation. Irradiation displacement damage levels in the bolts range from 15 to 41 displacements per atom. The goal of this project is to perform detailed microstructural and mechanical property characterization of BFBs following in-service exposures. The information from these bolts will be integral to the LWRS program initiatives in evaluating end of life microstructure and properties. Furthermore, valuable data will be obtained that can be incorporated into model predictions of long-term irradiation behavior and compared to results obtained in high flux experimental reactor conditions.

In this report, we present our latest study in FY21 on fracture toughness and FCGR testing of machined bend bar specimens from two harvested BFBs. The main finds are summarized as follows:

1) All four bend bar specimens exhibited stable ductile crack growth in fracture toughness testing.
2) The initiation fracture toughness J_q were similar and in the range of 40-60 kJ/m^2 for four bend bar specimens indicating the saturation of irradiation embrittlement.
3) Compared with the unirradiated condition, in-service neutron irradiation resulted in significant degradation of BFB fracture toughness, and the degradation was in line with current literature results.
4) Four bend bar specimens demonstrated similar FCGR behaviors manifested by a threshold stress intensity ΔK_{th}=11-13 MPa$\sqrt{m}$ and the stable crack growth region (i.e., Paris's law region).
5) The FCGR results fill the data gap of fatigue crack growth behavior of irradiated SS.

This page intentionally left blank

1. INTRODUCTION

As one of the pressurized water reactor (PWR) internal components, baffle-former bolts (BFBs) are subjected to significant mechanical stress and neutron irradiation from the reactor core during the plant operation. Over the long operation period, these conditions lead to potential degradation and reduced load-carrying capacity of the bolts, and life extension of existing PWRs would only cause more damage to the bolt material. Indeed, the BFB has been a particular concern for the nuclear industry since the first observation of failed bolts following the investigation of flow-induced vibration of fuel rods in elements on the core periphery observed in French 900 MW plants in the 1980s [1]. In the United States, the first degraded BFBs were observed in 1999. In support of evaluating long-term operational performance of materials used in core internal components, the Materials Research Pathway (MRP) under the U.S. Department of Energy (DOE) Light Water Reactor Sustainability (LWRS) Program has pursued the retrieval of aged structural components for the study of the microstructure, mechanical, and corrosion-related properties including stress corrosion cracking (SCC) and irradiation-assisted stress corrosion cracking (IASCC) initiation and growth. To this end, the MRP successfully harvested two high fluence BFBs from a Westinghouse two-loop downflow type PWR in 2016. In the same year, the two BFBs were received at the Westinghouse, Churchill, PA, facility for inspection and specimen fabrication. The fabrication was completed in 2017 with specimens shipped to Oak Ridge National Laboratory (ORNL) for further testing.

In this report, we present our latest study in FY21 on fracture toughness and fatigue crack growth rate (FCGR) testing of machined bend bar specimens from two harvested BFBs. The objective of this project is to provide information that is integral to evaluating end of life microstructure and properties as a benchmark of international models developed for predicting radiation-induced swelling, segregation, precipitation, and mechanical property degradation. Initial characterization focusing on microstructure for one harvested BFB and microhardness on both BFBs has been summarized in the FY19 milestone report for this project [2].

2. EXPERIMENTAL

2.1 MATERIALS

The retrieved BFBs are two of the highest fluence bolts available from the original type 347 austenitic stainless steel (SS) bolts used in the reactor. Both bolts showed no indication of cracking during the ultrasonic inspection and in visual inspection following removal from service. However, the bolts required a lower torque for removal from the baffle structure than the original torque specified during installation. Figure 2.1 shows images of the bolt heads of two retrieved BFBs. No indication of surface cracking was observed in the transition region between the shaft and head, although some surface debris scale flaked off from the bolt body. The shiny portion of the bolt head was due to electric discharge machining (EDM) when the bolts were removed from the baffle wall. The ID number for the bolts follows a 4-digit code with the first number being the quadrant location in the reactor, then the associated baffle plate number, the column location of the bolt associated with the particular baffle plate number, and finally the former plate location where the bolt originated. While the exact elemental compositions of the two retrieved BFBs are not available to us, Table 2.1 shows the compositions of three heats of type 347 SS used for the construction of the reactor in comparison with the material specification. The compositions of all three heats met the type 347 SS specification. However, based on the characterization results in FY19 for bolt #4416, it was found that the actual material for bolt #4416 was type 316 SS instead of type 347 SS due to lack of Nb and existence of Mo in the bolt. The same surprise was found in another bolt from Point Beach Unit 2, a Westinghouse two-loop PWR, as documented in an Electrical Power Research Institute (EPRI) report on hot cell testing of BFBs [4].

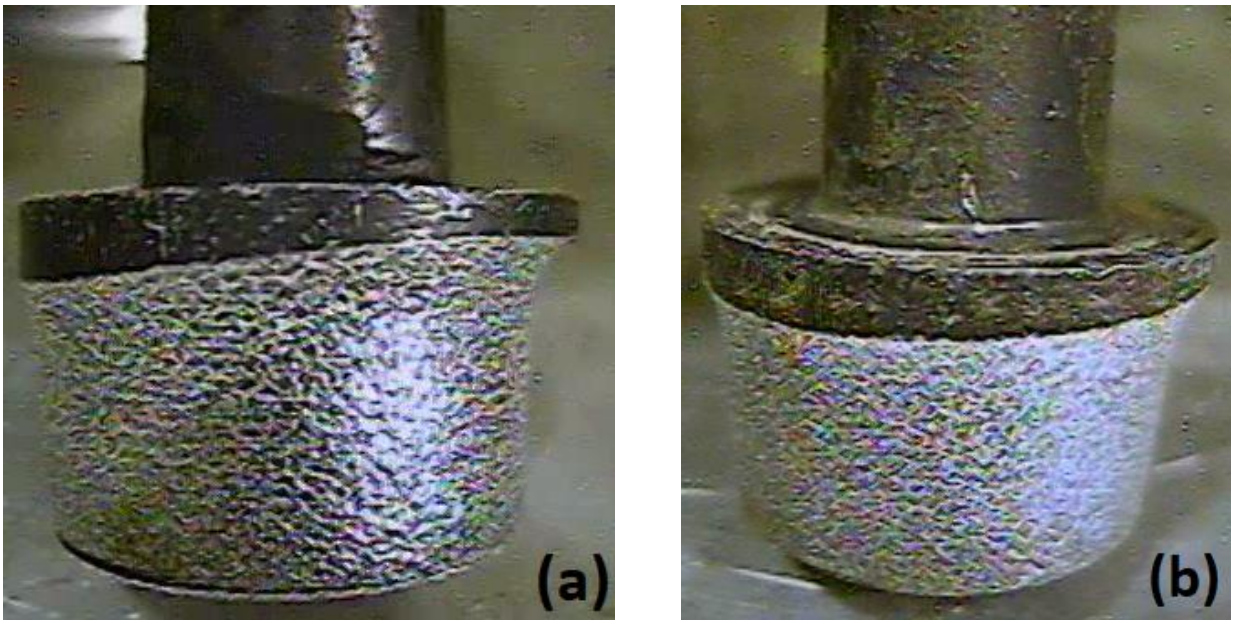

Figure 2.1 Images of bolt heads for bolt #4412 in (a) and bolt #4416 in (b) [3]

Table 2.1 Compositions of three heats of type 347 SS used for the construction of the reactor in comparison with material specification (wt%)

Element	Heat A	Heat B	Heat C	UNS S34700 spec.
Fe	Bal.	Bal.	Bal.	Bal.
Ni	10.46	10.68	9.80	9.00-13.00
Cr	18.10	17.95	18.64	17.00-19.00
Mn	1.63	1.34	1.83	2.00 max
Nb	0.96	0.70	0.81	10 x C min, 1.00 max
Si	0.75	0.55	0.75	1.00 max
C	0.05	0.06	0.07	0.08 max
P	0.03	0.03	0.023	0.045 max
S	0.026	0.02	0.018	0.03 max

Table 2.2 provides information on the range of fluences and estimated displacement damage along the length of the two bolts. The displacement damage values for the two bolts range from 15 to 41 displacements per atom (dpa) assuming a fluence to dpa conversion value of 6.7×10^{20} n/cm^2, E>1 MeV per dpa [5]. Other important information for the two retrieved bolts not available at the time of preparation of this report includes the irradiation temperature profile and flux both of which require more complicated modeling and calculation and can vary within each power cycle and from cycle to cycle. For instance, calculations [6] from Point Beach Unit 2, which is another Westinghouse two-loop type PWR, showed that the irradiation temperature and flux for a BFB from a region next to the bolt 4416 studied in this work varied in the range of 323-344°C and 7.5×10^{12}-1.8×10^{13} n/cm^2-sec (E>1 MeV) along the length of the bolt, respectively. Therefore, the value for a detailed calculation on irradiation temperature and flux of BFBs may be limited due to the large variation of those parameters during the lifetime of a BFB. It is worth noting that Point beach Unit 2 was originally a Westinghouse downflow two-loop PWR but was converted to upflow in Nov 1986 [6].

Table 2.2 Fluence and estimated displacement damage distributions for two retrieved BFBs

Bolt #	Fluence (10^{22} n/cm^2, E>1 MeV)/Estimated dpa		
	Head	Mid-shank	Mid-thread
4412	2.78/41	2.27/34	1.46/22
4416	1.91/29	1.56/23	1.00/15

The specimen machining plan and the schematic for specimen ID are shown in Figure 2.2 and Figure 2.3, respectively. For each BFB, four bend bar specimens and seven thin slice specimens have been machined. The bend bar specimens were used in the fracture toughness and fatigue crack growth rate studies of this report, whereas the thin slice specimens are planned for subscale tensile and microstructural analyses. Specimens were machined from different fluence regions of each bolt, allowing for studies of the effect of fluence on the microstructural and mechanical properties of BFBs. Three thin slice specimens were machined from the high-stress concentration region, i.e., the transition between the bolt head and shank, of each bolt to allow for further investigation of possible crack initiation sites. The IDs of bend bar specimens characterized in this study are summarized in Table 2.3 with

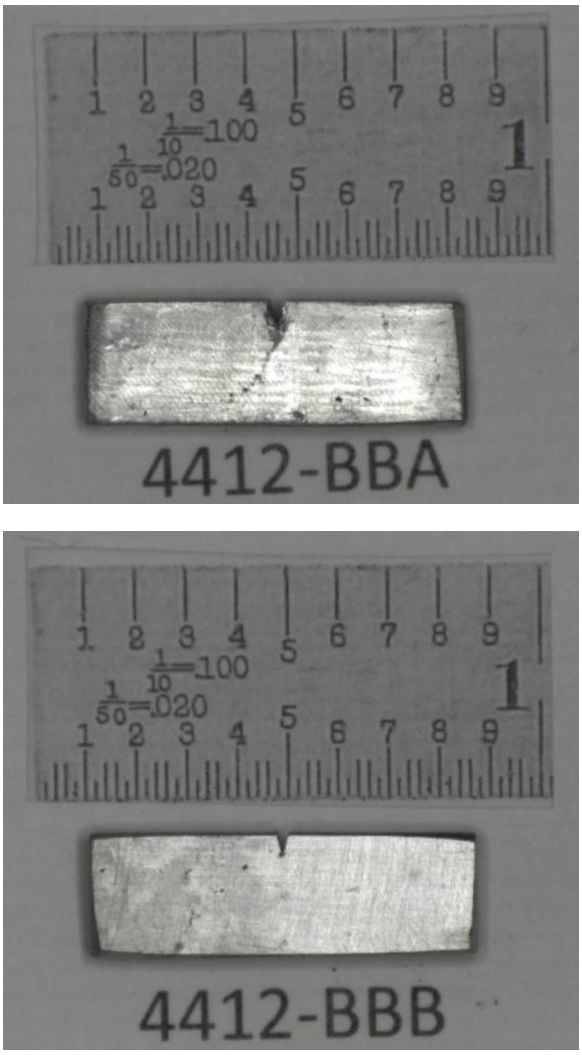

Figure 2.4 Images of machined bend bar specimens [2]

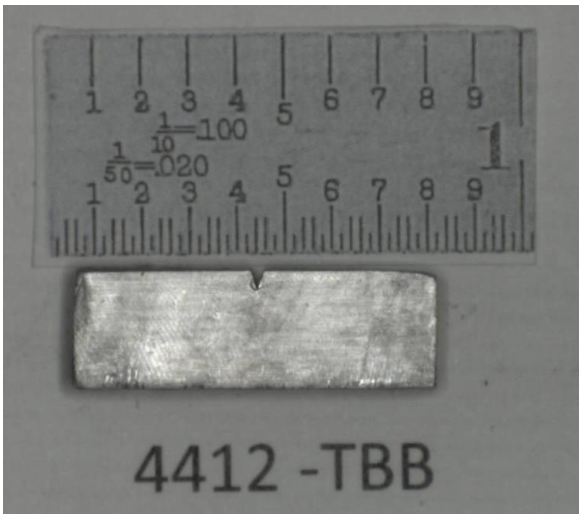

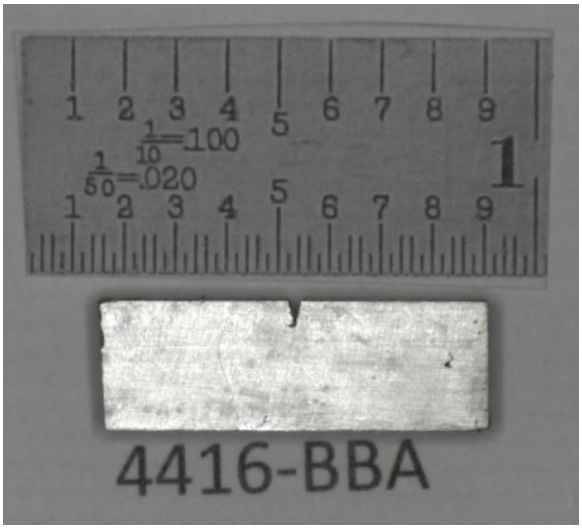

Figure 2.4 Cont.

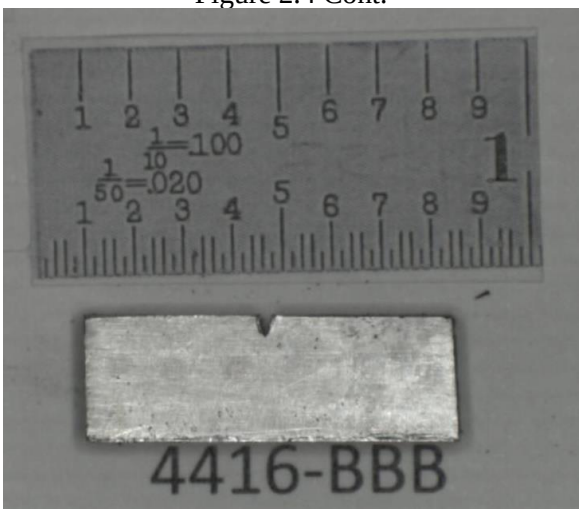

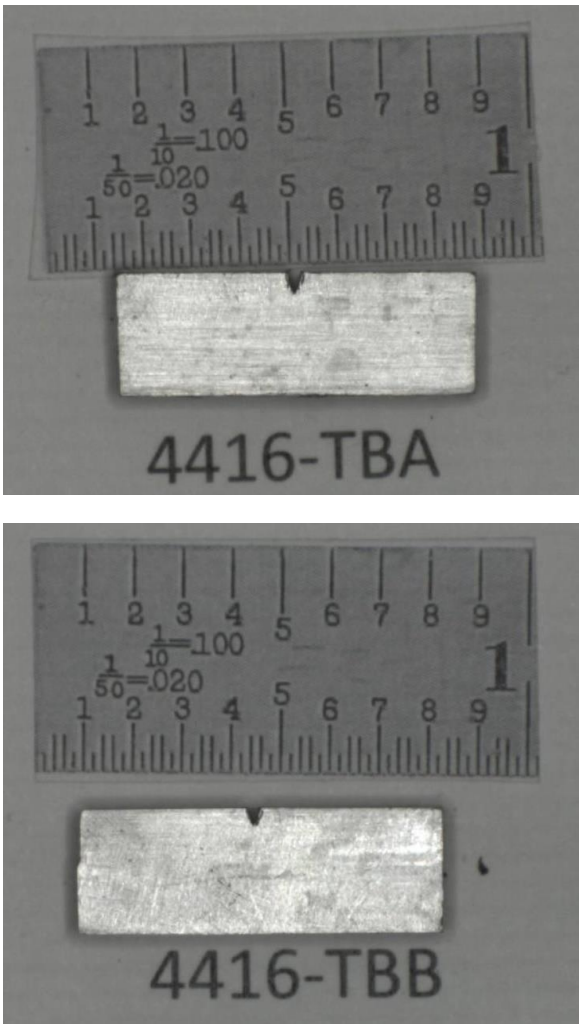

showing the images of each bend bar specimen. Small variations were observed for bend bar dimensions with the average dimension of 19.1 x 6.35 x 3.20 mm^3 (0.75 x 0.25 x 0.126 $inch^3$) with a span to width ratio of 2.42-2.63.

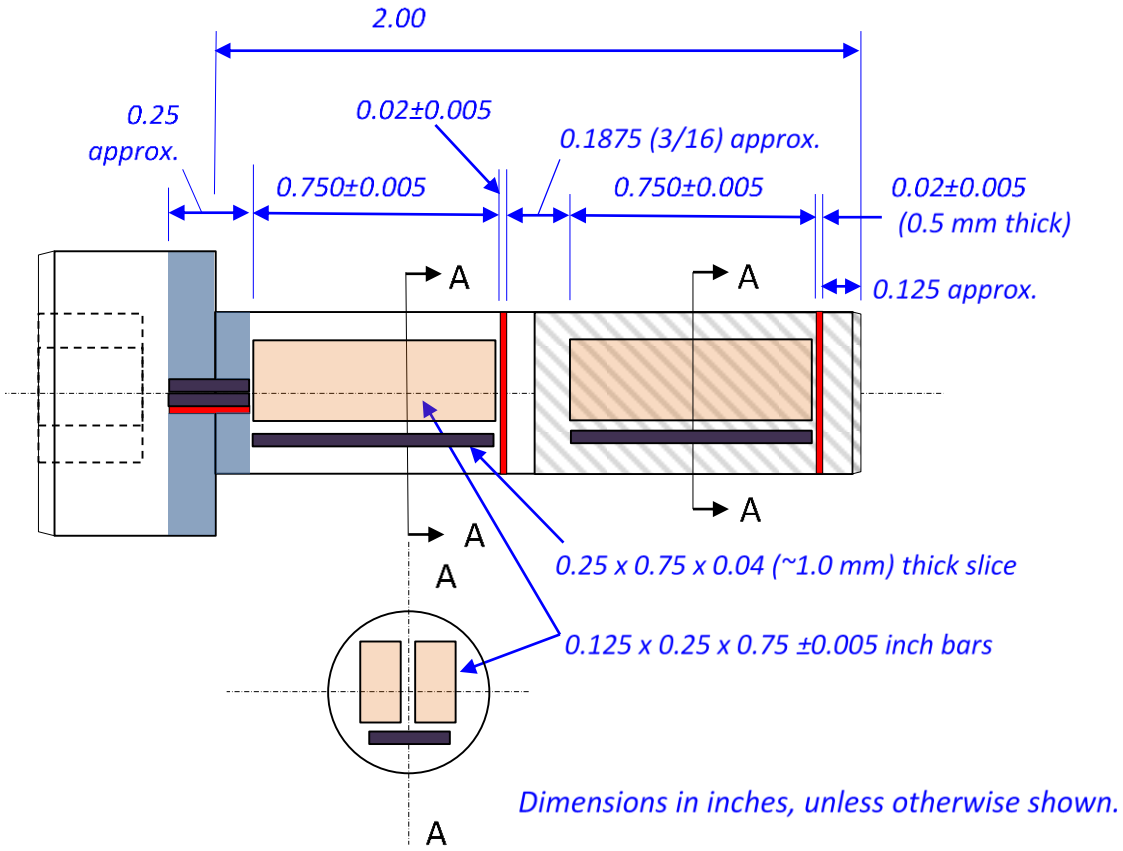

Figure 2.2 Machining diagram for the BFBs showing the color-coded sample types (red: 0.5 mm slices, black: 1.0 mm slices, light orange: bend bars, and light blue: remaining collar materials) [7]

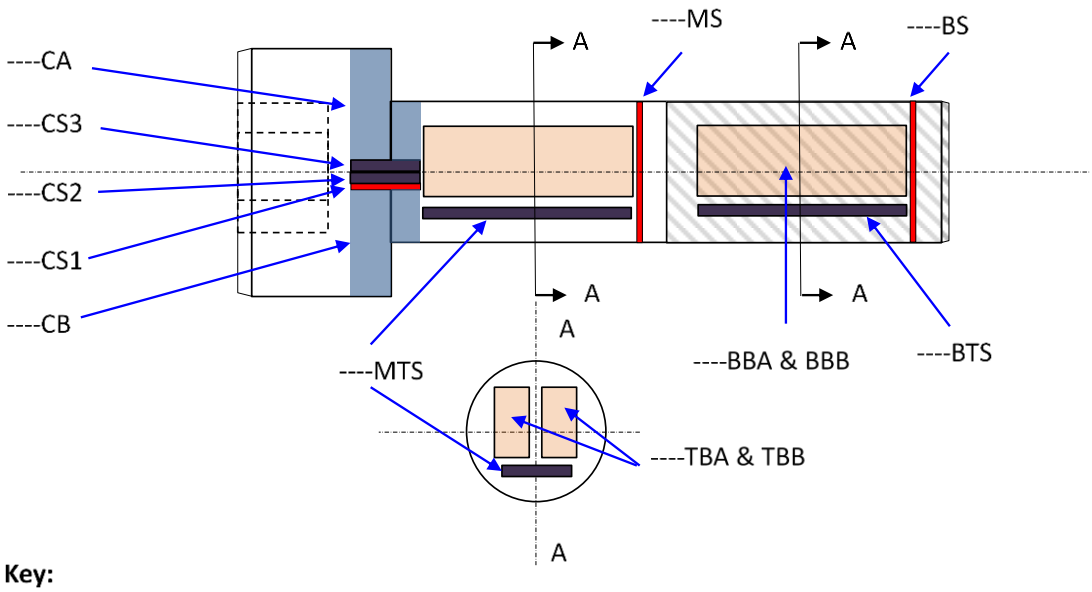

Key:
----: bolt number, **CS**: collar slice, **CA & CB**: remaining collar materials, **MS**: middle slice, **BS**: bottom slice, **MTS**: middle thick slice, **BTS**: bottom thick slice, **TBA & TBB**: top bend bar, **BBA & BBB**: bottom bend bar

Figure 2.3 Schematic for sample IDs from machined BFBs [7]

Table 2.3 IDs of bend bar specimens characterized in this study

Type of characterization	Bolt 4412		Bolt 4416	
	Mid-shank	Mid-thread	Mid-shank	Mid-thread
Fracture toughness	4412-TBA	4412-BBA	4416-TBA	4416-BBA
FCGR	4412-TBB	4412-BBB	4416-TBB	4416-BBB

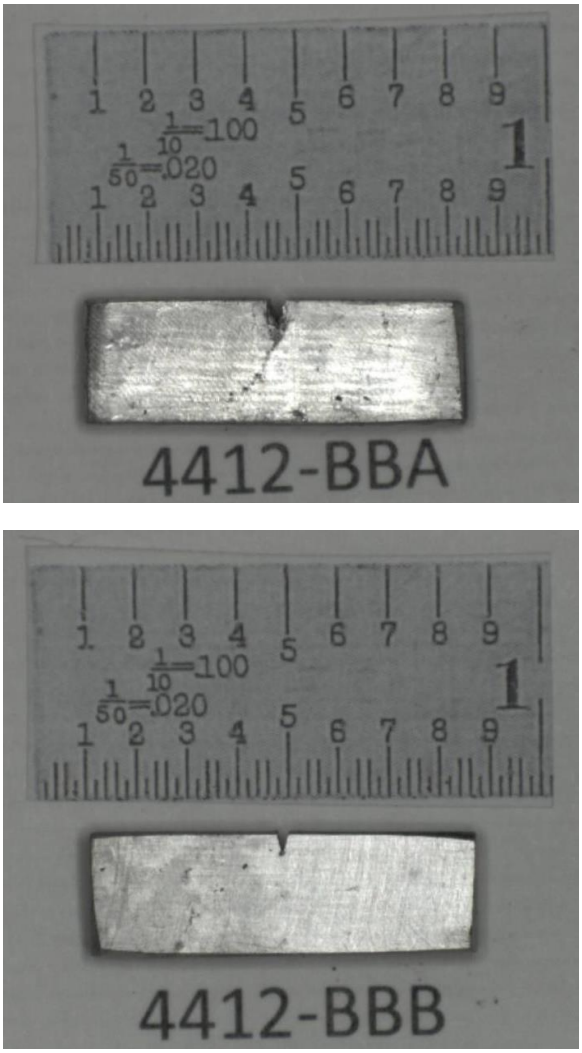

Figure 2.4 Images of machined bend bar specimens [2]

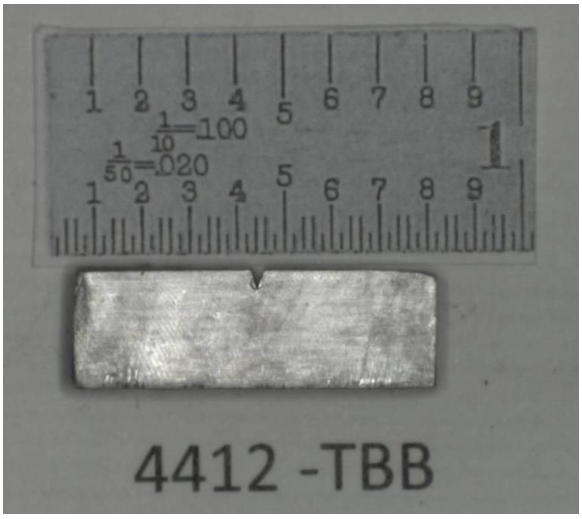

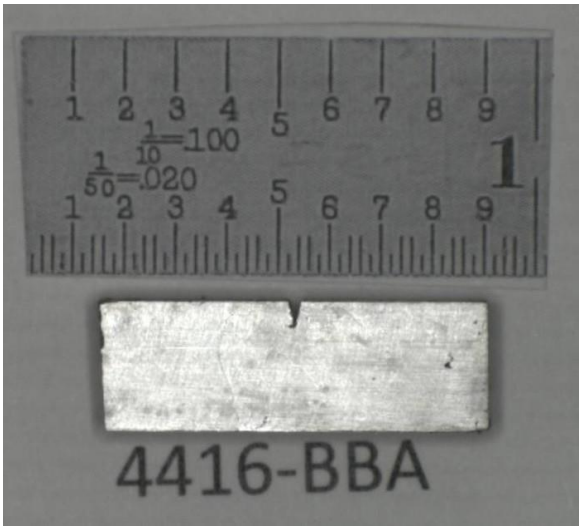

Figure 2.4 Cont.

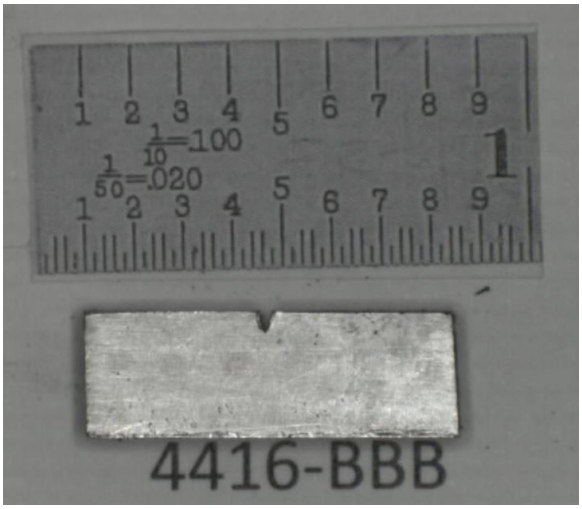

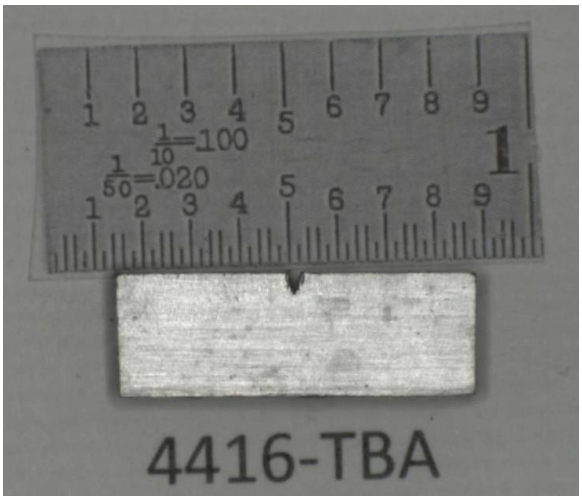

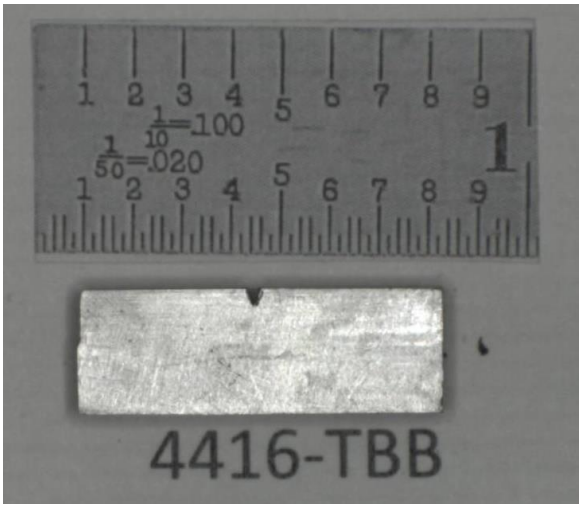

Figure 2.4 Cont.

2.2 FRACTURE TOUGHNESS AND FATIGUE CRACK GROWTH RATING TEST SETUP

Fracture toughness and FCGR testing, including fatigue precracking, were performed at the Irradiated Materials Examination and Testing Facility (IMET) of ORNL. A servo-hydraulic test frame, shown in Figure 2.5, was used for the testing. The frame has 444.8 kN load capacity and the load cell had a calibrated 22.25 kN capacity. Tests were performed at ambient temperature (22°C) in air.

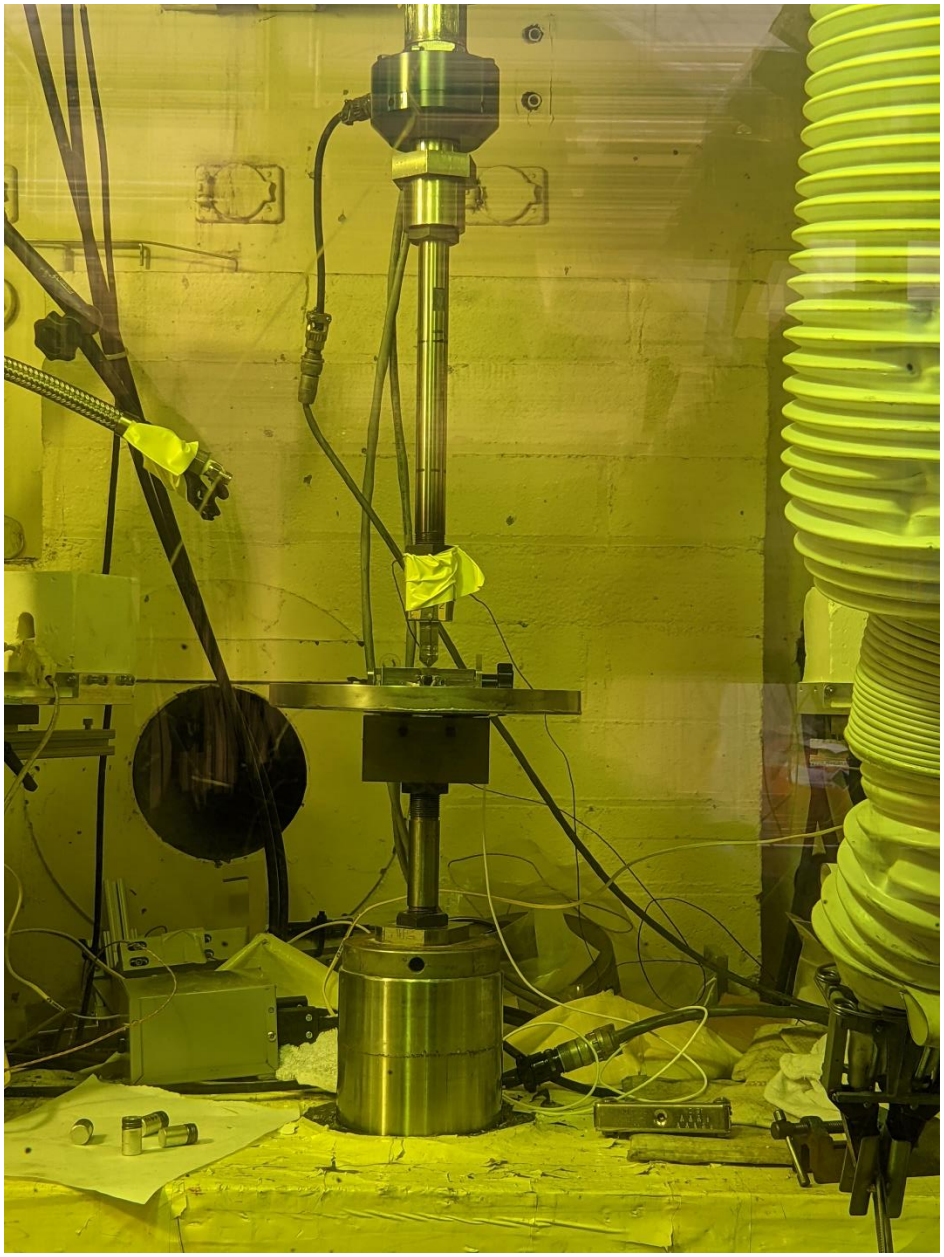

Figure 2.5 An MTS servohydraulic frame used in fracture toughness and FCGR testing

Due to the non-standard size of the bend bar specimen, we have designed a dedicated testing fixture to perform fracture toughness and FCGR testing. As shown in Figure 2.6, the deflection gauge attached to the specimen fixture center was used to measure the load-line displacement of the specimen. The sliding bar from the left side of the fixture was used to perform a coarse alignment of the specimen while the

threaded-hole knob from the right side was used to perform a fine adjustment of the specimen position so that the bend specimen was centered for the load pins and top indenter as shown in Figure 2.7.

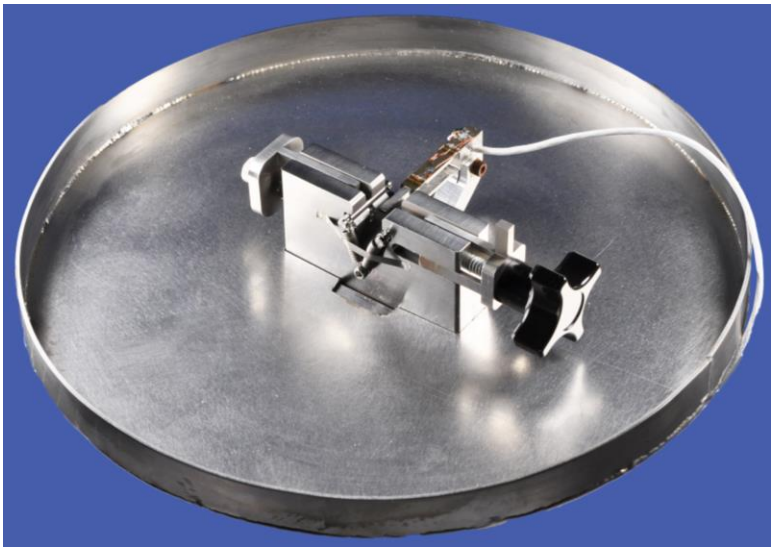

(a)

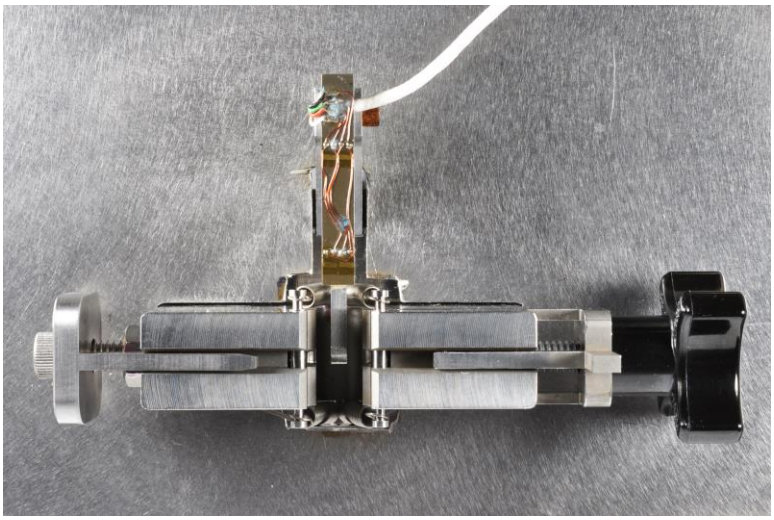

(b)

Figure 2.6 Bend bar test fixture: (a) isometric-view; (b) top-view

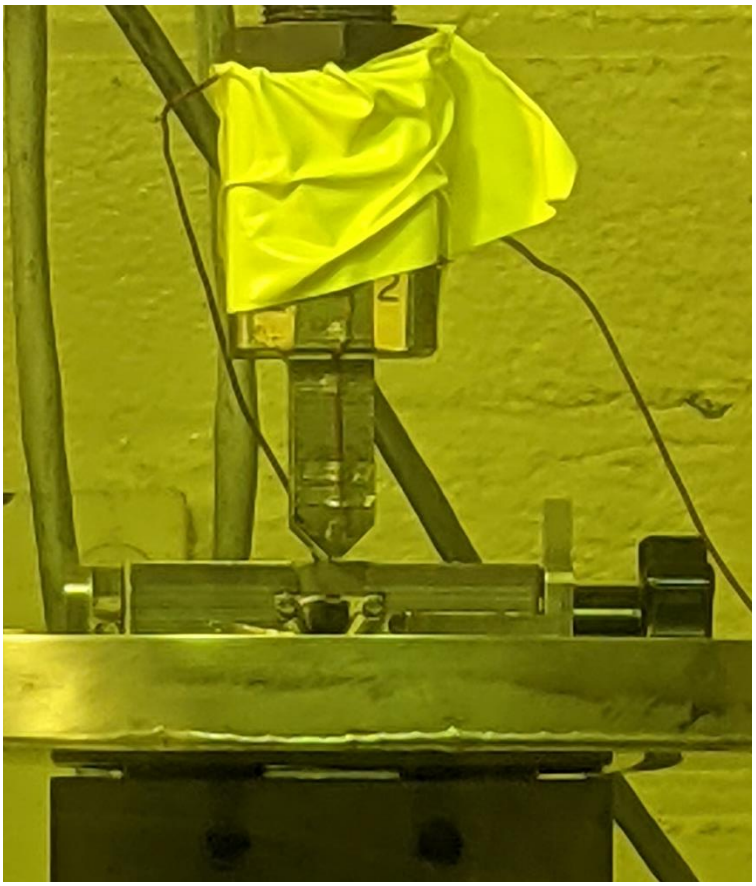

Figure 2.7 A bend bar specimen with notch center aligned in the test fixture

2.3 TESTING AND ANALYSIS PROCEDURES

2.3.1 Fracture Toughness Testing

Fracture toughness testing was performed according to the ASTM E1820 Standard Test Method for Measurement of Fracture Toughness [8]. Prior to fracture toughness testing, each bend bar specimen was fatigue precracked to a/W=0.5 (a: crack size, W: specimen width) using a sinusoidal waveform. The fatigue frequency was at ~10 Hz under a stress ratio R=0.1. Fatigue precracking was performed under stress intensity K control such that the maximum stress intensity K_{max} started around 24.17 MPa√m and decreased linearly as the crack grew and reached 19.45 MPa√m at the end of fatigue precracking. Figure 2.8 shows the typical K_{max} vs. a/W relationship in the fatigue precracking. The applied fatigue precracking stress intensity was within the allowable stress intensity limit per ASTM E1820 and also below the maximum allowable fatigue force (P_m) given by:

$$P_m = \frac{0.5Bb^2\sigma_Y}{S} \tag{1}$$

where:
B = specimen thickness,
b = length for the uncracked ligament,
σ_Y = average of material yield and tensile strengths,

S = span distance.

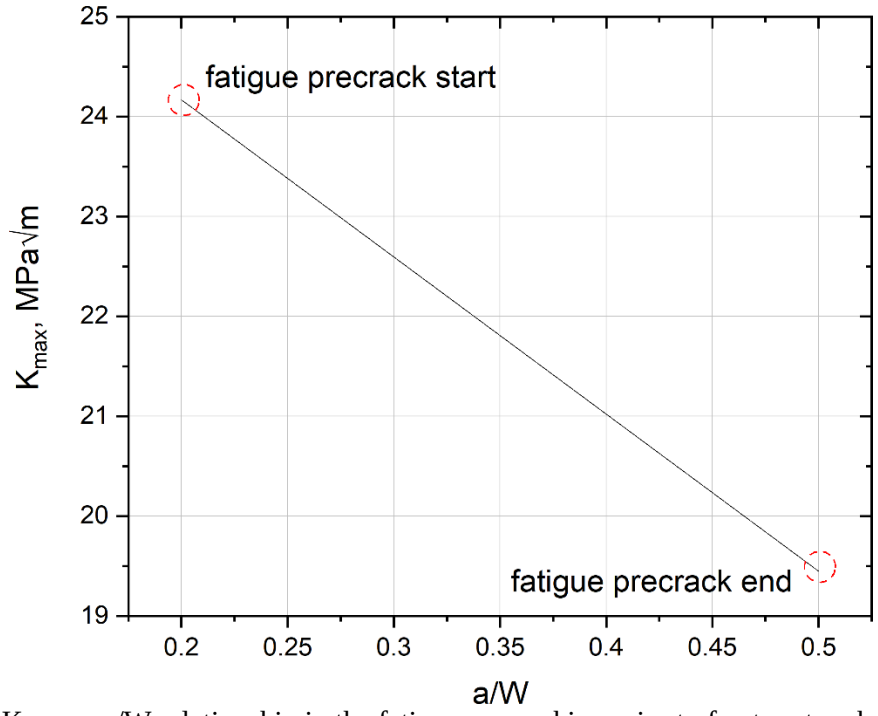

Figure 2.8 K_{max} vs. a/W relationship in the fatigue precracking prior to fracture toughness testing

During the fatigue precracking process, the load-line compliance at the machined notch of the bend bar specimen was used to calculate the real-time crack size. Due to the non-standard size of the bend bar specimen, i.e., span to width ratio S/W≠4, the equation from the ASTM E399 Standard Test Method for Linear-Elastic Plane-Strain Fracture Toughness of Metallic Materials [9] for the standard sized bend bar specimen cannot be used in such calculation. Therefore, we adopted the method highlighted in the book of Wallin [10] and derived a revised equation to convert the load-line compliance to the real-time crack size as in:

$$a/W = -1.5396 + 36.149U - 165.401U^2 - 191.204U^3 + 2626.017U^4 - 4496.344U^5$$
$$U = 1/\{[dE(BB_n)^{1/2}/P]^{1/2} + 1\} \quad (2)$$

where:
a = crack length,
d/P = measured load-line compliance,
E = material Young's modulus (200 GPa),
B_n = specimen net thickness (equals B for non-side grooved bend bar specimen),
B = specimen thickness.

After fatigue precracking, fracture toughness testing was performed based on the ASTM E1820 standard, and the J-integral vs. crack growth resistance (J-R) curve analysis was performed based on the Normalization method described in the same standard. We have developed an in-house analysis procedure for applying the Normalization method and have applied it for a variety of materials (including stainless steels) and testing conditions with satisfactory results [11-12]. Similar to Eq. 2, the stress intensity K and load-line compliance calculation C_Δ was adjusted based on the following two equations to count for the non-standard specimen size [10, 13]:

$$K = \frac{P \cdot S}{B \cdot W^{3/2}} \cdot f(\frac{a}{W}) \cdot \left\{1 + (1 - \frac{4W}{S}) \left[0.08\frac{b}{W} + 0.24(\frac{b}{W})^2 - 0.28(\frac{b}{W})^3\right]\right\}$$
$$f(\frac{a}{W}) = \frac{3 \cdot \sqrt{\frac{a}{W}} \cdot \left[1.99 - \frac{a}{W} \cdot (1 - \frac{a}{W}) \cdot (2.15 - 3.93 \cdot \frac{a}{W} + 2.7 \cdot (\frac{a}{W})^2)\right]}{2 \cdot (1 + 2 \cdot \frac{a}{W}) \cdot (1 - \frac{a}{W})^{3/2}} \quad (3)$$

$$EB_eC_\Delta = (\frac{S}{W})^3 \cdot \left[0.25 + 0.6 \cdot (1 + \nu) \cdot (\frac{W}{S})^2\right] + (\frac{S}{W})^2 \cdot \frac{(a/W)^2}{(1 - a/W)^2} \cdot$$
$$\left[8.9 - 33.717 \cdot \frac{a}{W} + 79.616 \cdot (\frac{a}{W})^2 - 112.952 \cdot (\frac{a}{W})^3 + 84.815 \cdot (\frac{a}{W})^4 - 25.672 \cdot (\frac{a}{W})^5\right] \cdot \left\{1 + (1 - \frac{4W}{S}) \cdot g(b/W)\right\} \quad (4)$$
$$g(b/W) = 0.475\frac{b}{W} - 0.458(\frac{b}{W})^2 + 0.033(\frac{b}{W})^3$$

where:
P = load,
B_e = effective thickness, equals to $B-(B-B_N)^2/B$,
ν = Poisson's ratio (0.3).

Upon completion of fracture toughness testing, each bend bar specimen was heat-tinted on a hot plate at 320 °C for a few hours to mark the final crack size of fracture toughness testing.

2.3.2 FCGR

FCGR testing was performed according to the ASTM E647 Standard Test Method for Measurement of Fatigue Crack Growth Rates [14]. Similar to fracture toughness testing, fatigue precracking was performed prior to the FCGR testing to create a sharp starting crack. The fatigue frequency was at ~10 Hz under a stress ratio R=0.1. The same K_{max} vs. a/W slope highlighted in Figure 2.8 was used in fatigue precracking until the crack size reached 2.02 mm to reserve uncracked ligament for the following FCGR testing.

Depending on the individual bend bar specimen, a constant force amplitude in the range of 845-979 N was applied during FCGR. The fatigue frequency was at ~10 Hz under a stress ratio R=0.1. As the crack size grew, the applied stress intensity K also increased, and we can measure the approximate threshold stress intensity value for initiating the crack growth (ΔK_{th}) as well as Paris's law region slope for the rate of crack growth (da/dN) vs. the range of stress intensity (ΔK). The test was stopped when the applied stress intensity reached the allowable stress intensity K_{max} defined in the following equation from the ASTM E647 standard to ensure the loading was predominately elastic:

$$(W - a) \geq (4/\pi)(K_{max}/\sigma_{YS})^2 \quad (5)$$

where:
σ_{YS} = material yield strengths.

Similar to fracture toughness testing, the applied stress intensity K was adjusted using Eq. 3 to account for the non-standard specimen size. Linear visual correction using the measured initial and final crack sizes in FCGR was also applied. After fatigue precracking, each bend bar specimen was heat tinted on a hot plate at 340 °C for a few hours to mark the final crack size of FCGR testing.

3. RESULTS AND DISCUSSION

3.1 FRACTURE TOUGHNESS

All four bend bar specimens exhibited stable ductile crack growth in fracture toughness testing. This can be shown from the load-displacement curves and fracture surface images after testing (Figure 3.1). The load decreased smoothly after passing the maximum load and dimpled fracture morphology was observed from the fracture surface.

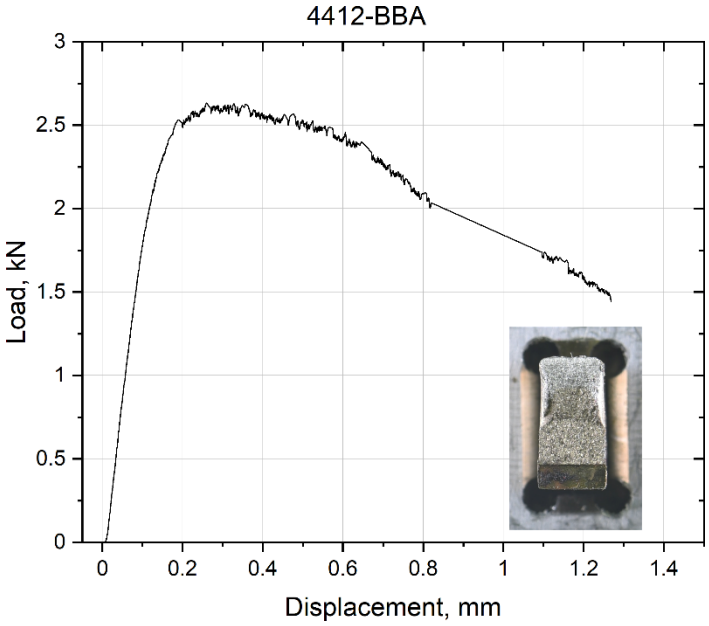

(a)

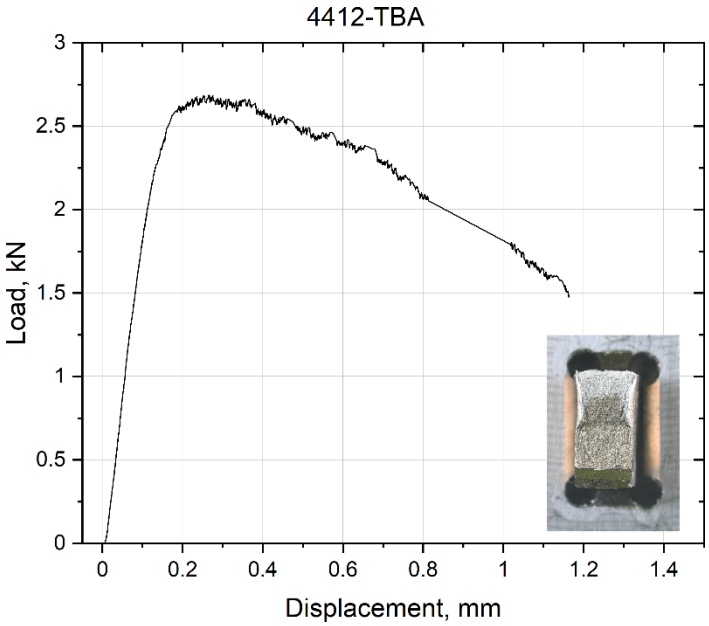

(b)

Figure 3.1 Load-displacement curves and fracture surface images for (a) 4412-BBA, (b) 4412-TBA, (c) 4416-BBA, (d) 4416-TBA.

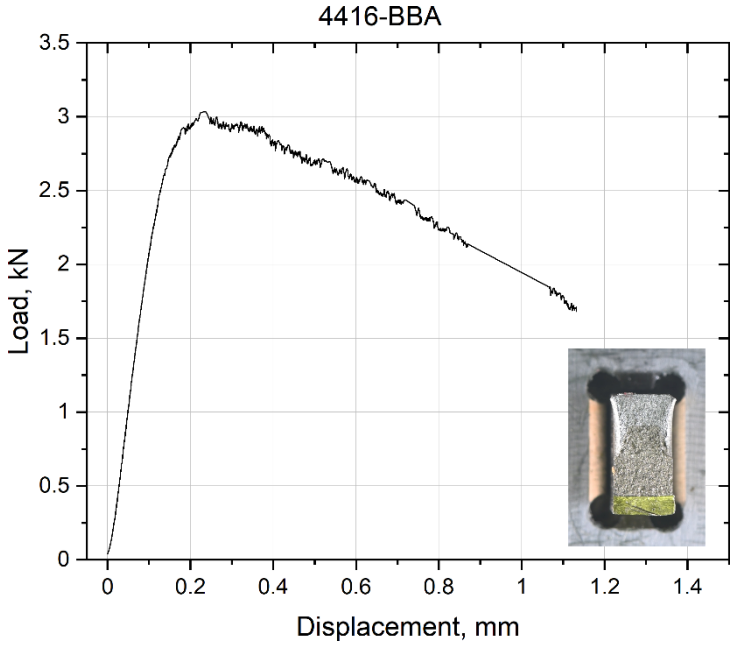

(c)

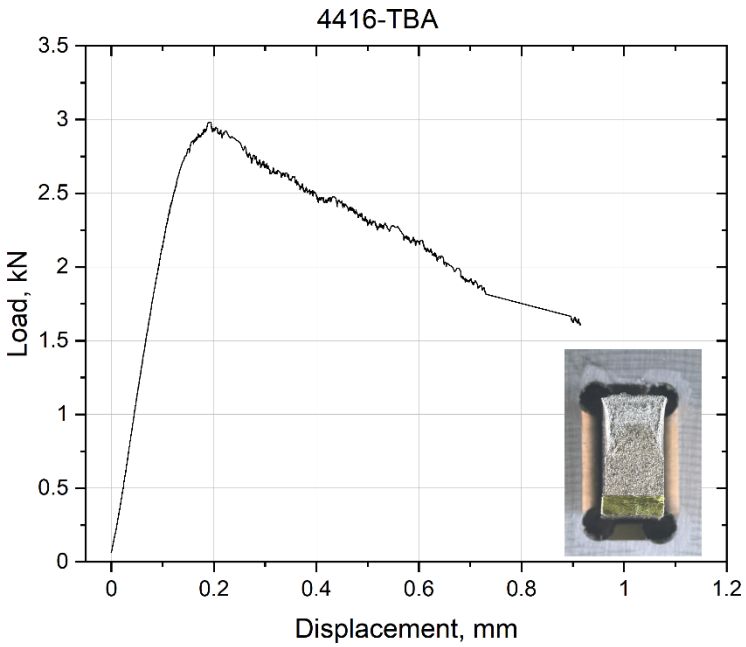

(d)

Figure 3.1 Cont.

The corresponding J-R curves derived from the Normalization method are shown in Figure 3.2. Among all four tested specimens, a similar trend in the J-R curve can be observed: the initiation fracture toughness J_q was fairly low; after crack initiation, the additional driving force was needed for the crack to propagate and the resistance for further crack growth significantly increased when the crack extension Δa reached ~0.7 mm. This seems to contradict the results reported in Ref. [5] where most J-R curves did not show a significant increase in the slope. While further study is needed to understand the cause, possible explanations include the specimen size effect, non-standard span to width ratio, and issues with the test

fixture. However, all these factors should not affect the initiation fracture toughness determined in this study.

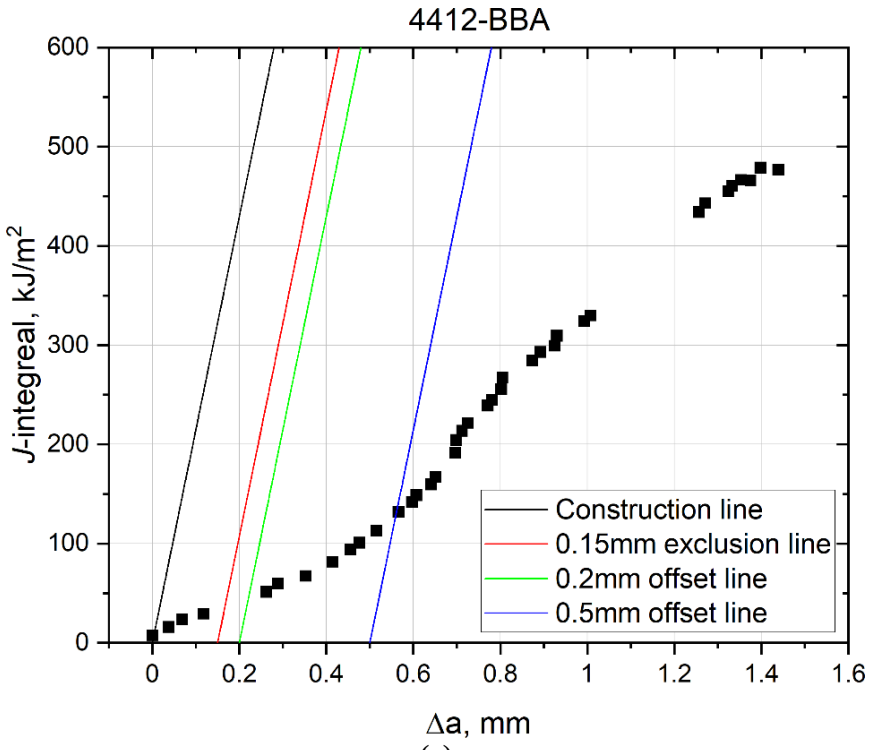

(a)

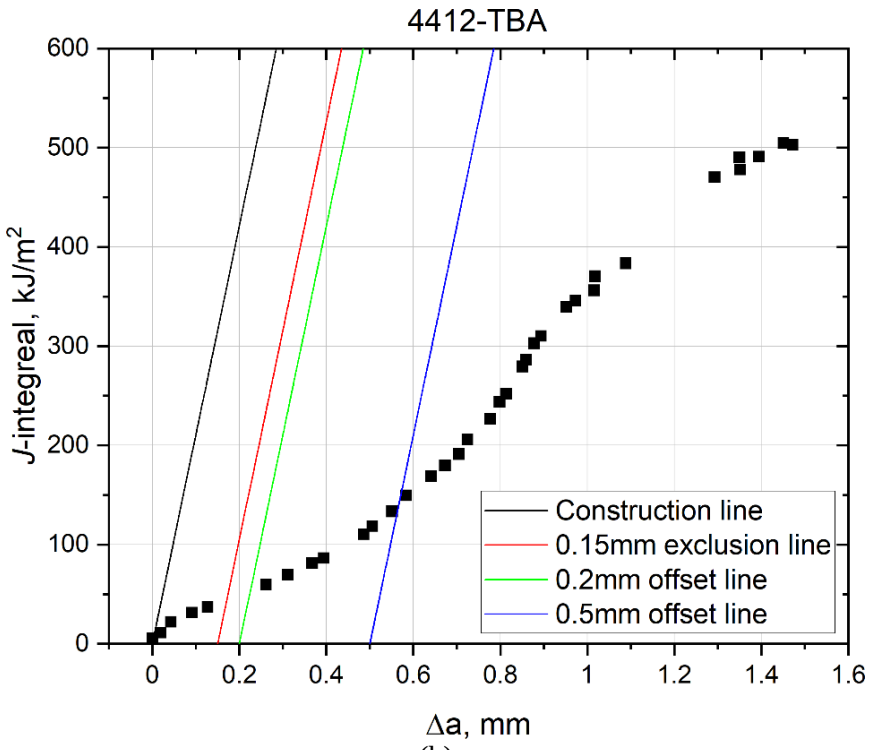

(b)

Figure 3.2 J-R curves for (a) 4412-BBA, (b) 4412-TBA, (c) 4416-BBA, (d) 4416-TBA.

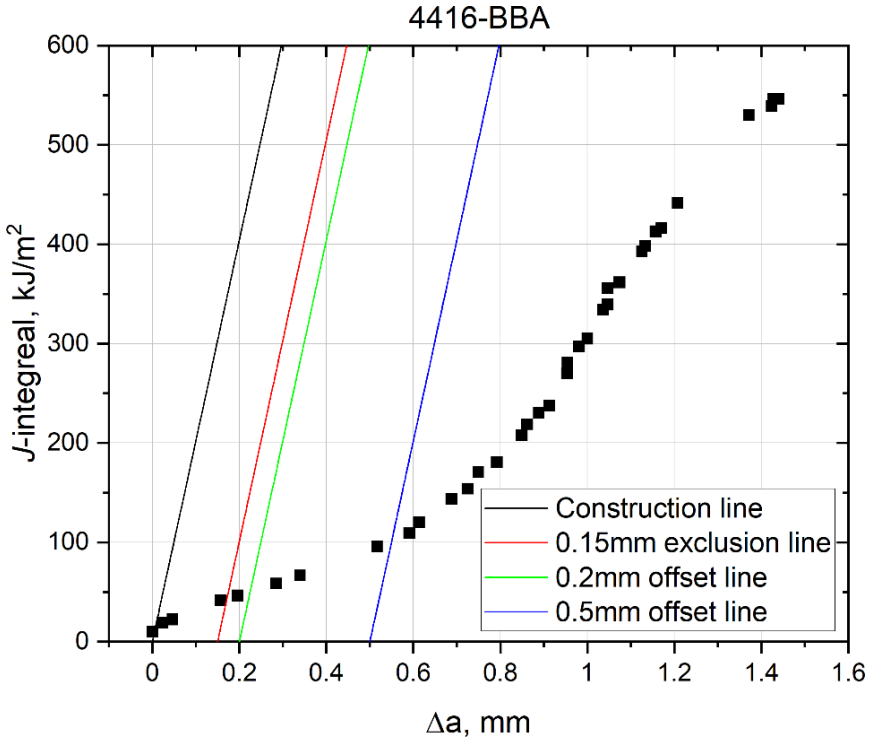

(c)

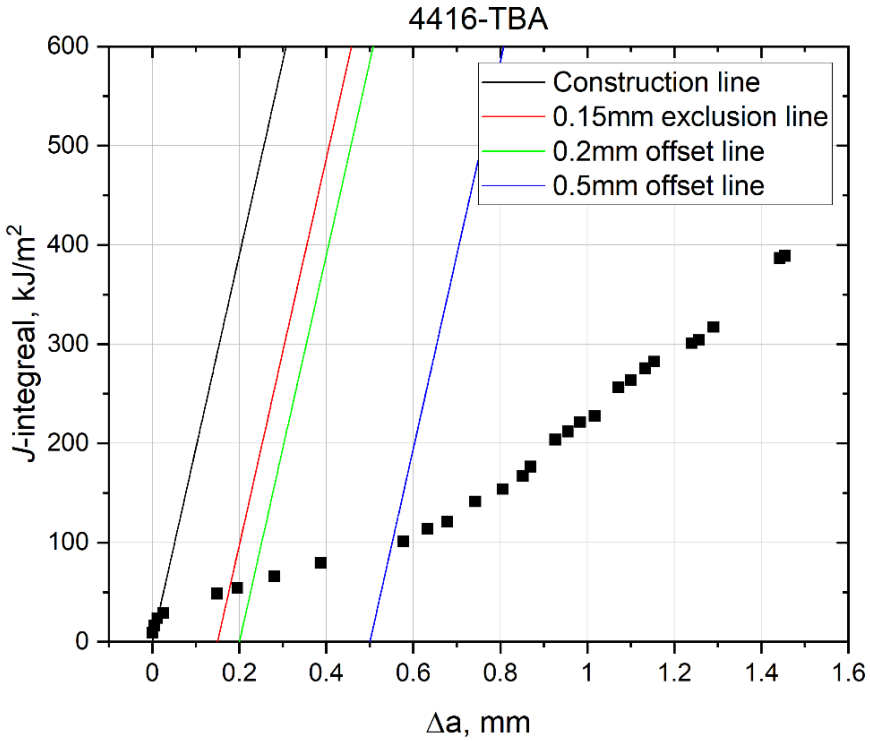

(d)

Figure 3.2 Cont.

As shown in Figure 3.3, the initiation fracture toughness J_q of four bend bar specimens were quite similar in the range of 40-60 kJ/m^2 and the small difference observed is within the measurement uncertainty

in J-R curve testing. Indeed, Table 2.2 shows the lowest irradiation damage for both bolts was approximately 15 dpa which already exceeded the saturation dose level (10 dpa based on Ref. [5]) for irradiation embrittlement. It is worth noting that wrought SS materials used for making both bolts have a category III initiation fracture toughness between 169 and 1660 kJ/m^2 at the unirradiated condition [5] (green shaded region in Figure 3.3). Compared with the post-irradiation initiation fracture toughness, the in-service neutron irradiation resulted in significant degradation of materials fracture toughness. This is in line with reports reported for both light water reactors (LWRs) and fast reactors [5].

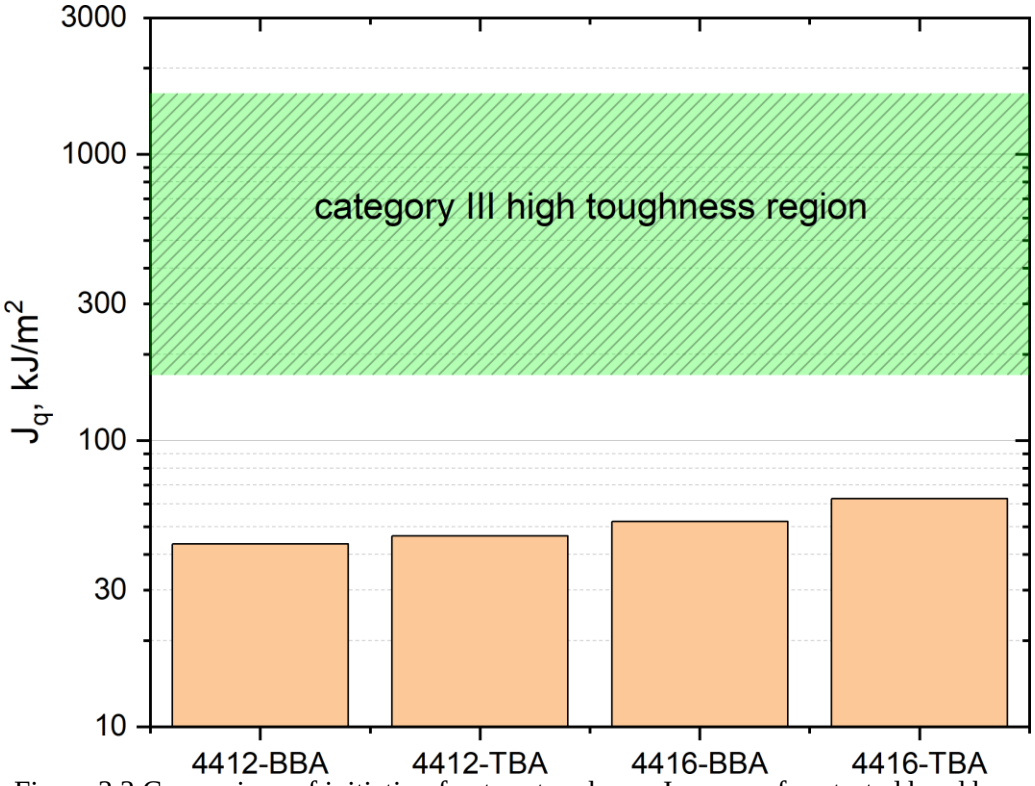

Figure 3.3 Comparison of initiation fracture toughness J_q among four tested bend bars

Figure 3.4 evaluates if the initiation fracture toughness results in this work can be bounded by the initiation fracture toughness lower bound trend curve defined in the Nuclear Regulatory Report NUREG/CR-7027[5]. The trend curve was developed for a variety of wrought austenitic SS, cast SS, and weld metals and can represent the worst-case scenario. All data points from this work are above the trend line indicating our results are reasonable and within the lower bound of the existing database.

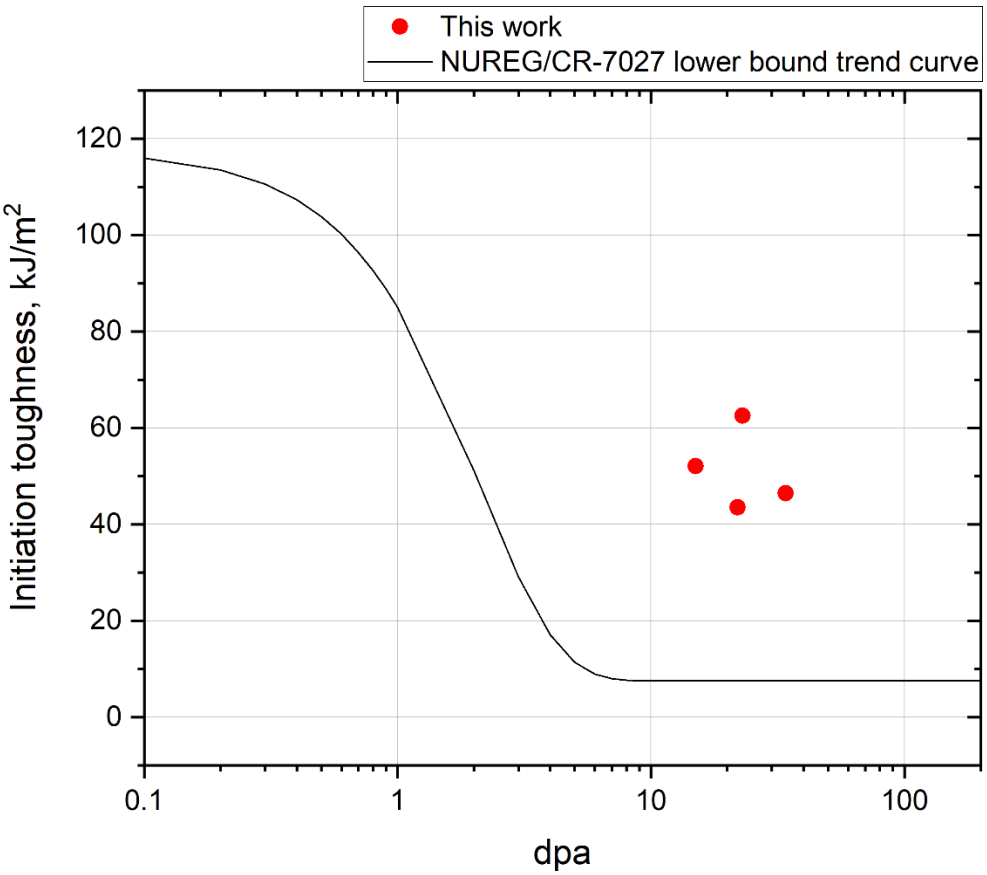

Figure 3.4 Comparison of NUREG/CR-7027 [5] low bound trend curve vs. the

3.2 FATIGUE CRACK GROWTH RATE

In FCGR testing, four bend bar specimens demonstrated similar behavior. The relationships between the crack growth rate per cycle, da/dN, and the stress intensity range ($\Delta K = K_{max} - K_{min}$) are shown in Figure 3.5. At around ΔK_{th}=11-13 MPa$\sqrt{m}$, crack initiated from the fatigue precracking end and started to grow. Afterward, the test gradually transitioned into Paris's law region [15], i.e., $da/dN=C\Delta K^m$ where C and m are materials coefficients and also depend on the testing environment, fatigue frequency, temperature, stress ratio, etc. The threshold stress intensity ΔK_{th} and Paris's law region slope m were analyzed and summarized in Table 3.1. At the time of preparation of this report and to the best of our knowledge, the FCGR results for irradiated SS are not available in the literature. Therefore, results from our current study fill the current data gap in this area.

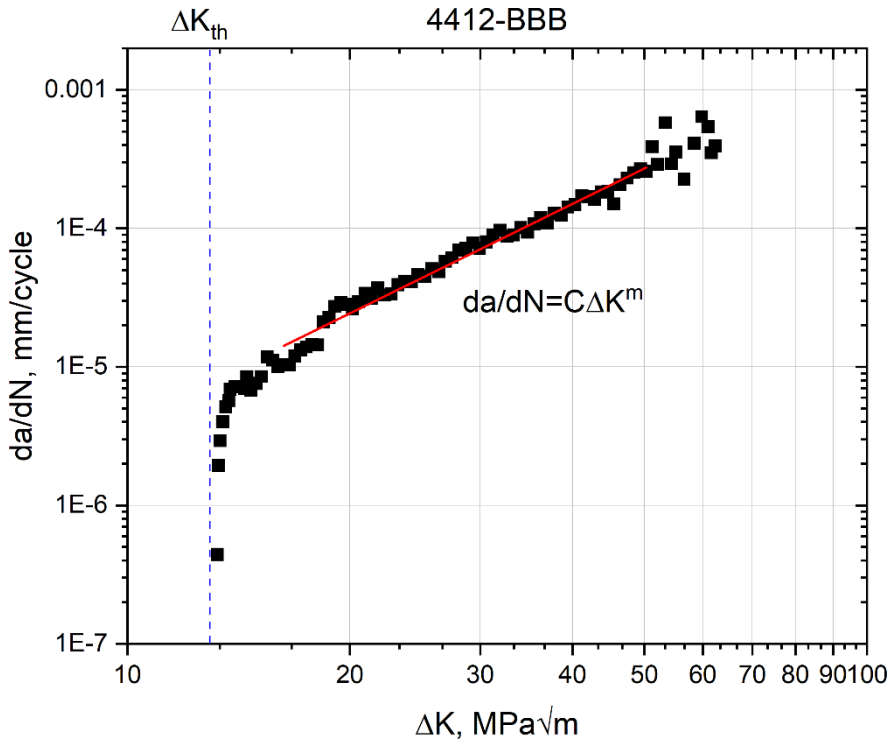

(a)

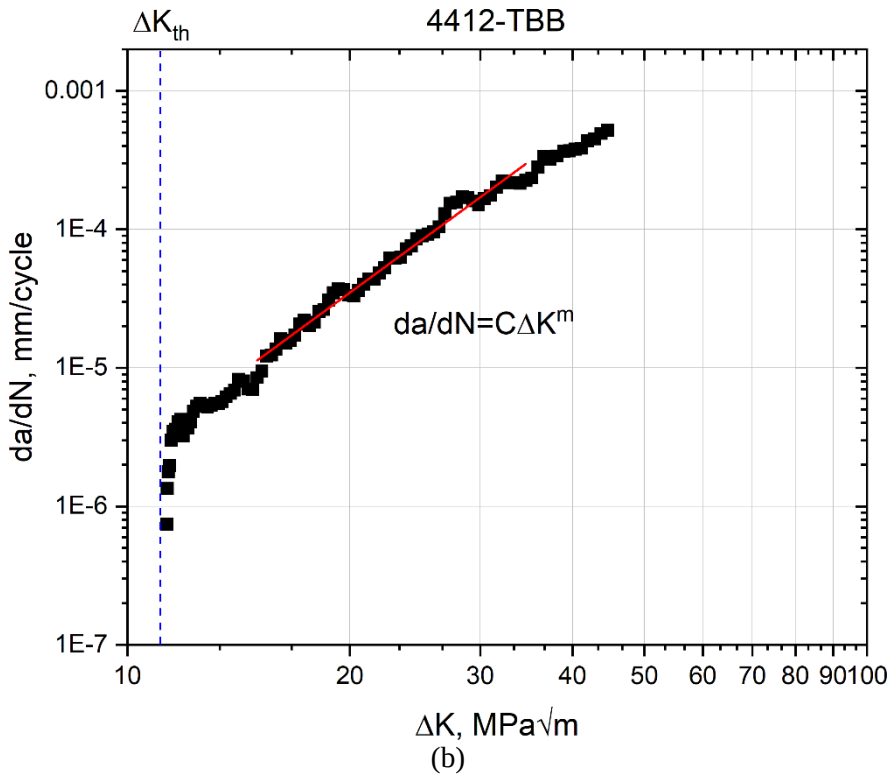

(b)

Figure 3.5 Relationship between da/dN and ΔK for (a) 4412-BBB, (b) 4412-TBB, (c) 4416-BBB, (d) 4416-TBB.

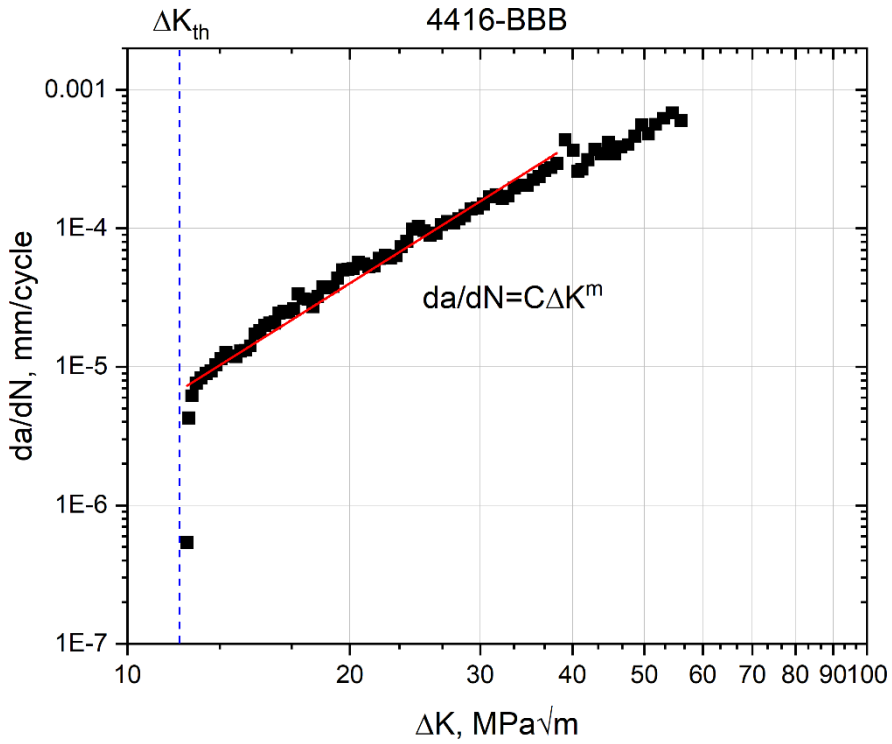

(c)

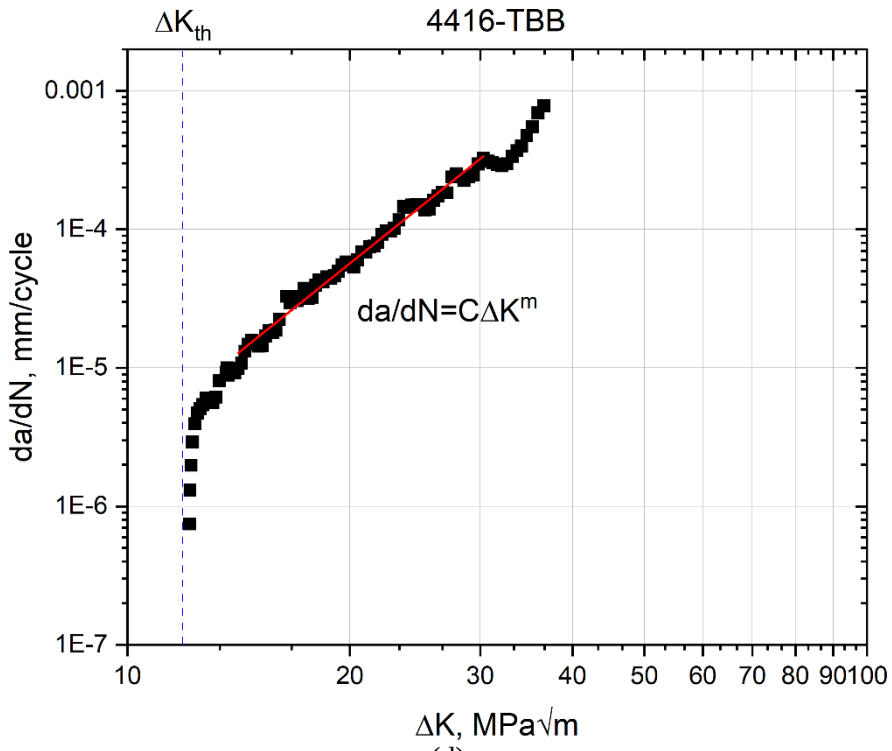

(d)

Figure 3.5 Cont.

Table 3.1 FCGR threshold stress intensity and Paris's law region slope analysis

Specimen ID	ΔK_{th} (MPa$\sqrt{m}$)	m	Fitting R^2
4412-BBB	12.9	2.63	0.976
4412-TBB	11.1	3.91	0.984
4416-BBB	11.8	3.36	0.914
4416-TBB	11.9	4.28	0.986

4. CONCLUSIONS

In this report, we present our latest study in FY21 on fracture toughness and FCGR testing of machined bend bar specimens from two harvested BFBs. The objective of this project is to provide information that is integral to evaluating end of life microstructure and properties as a benchmark of international models developed for predicting radiation-induced swelling, segregation, precipitation, and mechanical property degradation. The main finds are summarized as follows:

1) All four bend bar specimens exhibited stable ductile crack growth in fracture toughness testing.
2) The initiation fracture toughness J_q were similar and in the range of 40-60 kJ/m^2 for four bend bar specimens indicating the saturation of irradiation embrittlement.
3) Compared with the unirradiated condition, in-service neutron irradiation resulted in significant degradation of BFB fracture toughness, and the degradation was in line with current literature results.
4) Four bend bar specimens demonstrated similar FCGR behaviors manifested by a threshold stress intensity ΔK_{th}=11-13 MPa$\sqrt{m}$ and the stable crack growth region (i.e., Paris's law region).
5) The FCGR results fill the data gap of fatigue crack growth behavior of irradiated SS.

5. REFERENCES

[1] IAEA Technical Report, Stress Corrosion Cracking in Light Water Reactors: Good Practices and Lessons Learned, report number NP-T-3.13, International Atomic Energy Association, Vienna, Austria 2011.

[2] X. CHEN, T. Chen, C.M Parish, T. Graening, M.A. Sokolov, K. J. Leonard, Post-Irradiation Examination of High Fluence Baffle-Former Bolts Retrieved from a Westinghouse Two-Loop Downflow Type PWR, ORNL/TM-2019/1251, July 31, 2019.

[3] X. CHEN, K. J. LEONARD, M. A. SOKOLOV, M. A. BURKE, M. N. GUSSEV, S. R. CLARK, Specimen Fabrication from Two High Fluence Ginna Baffle Bolts, ORNL/TM-2017/455, August 25, 2017.

[4] H. T. Tang, Materials Reliability Program Hot Cell Testing of Baffle/Former Bolts Removed from Two Lead PWR Plants (MRP-51), report number 1003069, EPRI technical report (2001).

[5] O. K. CHOPRA, Degradation of LWR Core Internal Materials due to Neutron Irradiation, NUREG/CR-7027 (2010).

[6] H. T. TANG, Materials Reliability Program Determination of Operating Parameters of Extracted Bolts (MRP-52), report number 1003076, EPRI technical report (2001).

[7] K. J. LEONARD, M. A. SOKOLOV, M. N. GUSSEV, Post-Service Examination of PWR Baffle Bolts, Part I. Examination and Test Plan, Oak Ridge National Laboratory Report, ORNL/LTR-2015/193, April 30, 2015.

[8] ASTM E1820-20b, Standard Test Method for Measurement of Fracture Toughness, ASTM International, West Conshohocken, PA, 2020, www.astm.org

[9] ASTM E399-20a, Standard Test Method for Linear-Elastic Plane-Strain Fracture Toughness of Metallic Materials, ASTM International, West Conshohocken, PA, 2020, www.astm.org

[10] K. Wallin, Fracture toughness of engineering materials: Estimation and application. EMAS publishing, 2011.

[11] X. Chen, R. K. Nanstad, M. A. Sokolov, E. T. Manneschmidt, Determining ductile fracture toughness in metals. Advanced Materials & Processes, 172, 19-23, 2014.

[12] A. E. Linares, L. Clowers, X. Chen, M. A. Sokolov, R. K. Nanstad, Using Automated JR Curve Analysis Software to Simplify Testing and Save Time, ADVANCED MATERIALS & PROCESSES, 177(3), 6-6, 2019

[13] A. Bakker, COMPATIBLE COMPLIANCE AND STRESS INTENSITY EXPRESSIONS FOR THE STANDARD THREE-POINT BEND SPECIMEN. Fatigue & Fracture of Engineering Materials & Structures, 13(2), 145-154, 199

[14] ASTM E647-15e1, Standard Test Method for Measurement of Fatigue Crack Growth Rates, ASTM International, West Conshohocken, PA, 2015, www.astm.org

[15] P. C. Paris, F. Erdogan, A critical analysis of crack propagation laws, Journal of Basic Engineering. 18 (4): 528–534, 1963